Available online at www.sciencedirect.com

ScienceDirect

Scripta Materialia 89 (2014) 29–32

Scripta MATERIALIA

www.elsevier.com/locate/scriptamat

Micromagnetic simulations on the grain size dependence of coercivity in anisotropic Nd–Fe–B sintered magnets

H. Sepehri-Amin,[a,*] T. Ohkubo,[a] M. Gruber,[a] T. Schrefl[b] and K. Hono[a]

[a] *Elements Strategy Initiative Center for Magnetic Materials, National Institute for Materials Science, Tsukuba 305-0047, Japan*
[b] *St Pölten University of Applied Science, St Pölten, Austria*

Received 22 April 2014; revised 19 June 2014; accepted 21 June 2014
Available online 2 July 2014

Micromagnetic simulations of magnetization reversals of Nd–Fe–B anisotropic magnets with exchange-coupled grains demonstrate that the local demagnetization factor decreases as the grain size is reduced. This explains the higher coercivity and the lower temperature dependence of coercivity in magnets with smaller grain sizes. When a fraction of $Nd_2Fe_{14}B$ grains become a single domain state for average grain sizes <1 μm, a higher magnetic field is needed to magnetize them, giving rise to a two-step initial magnetization curve.

Keywords: Micromagnetic simulations; Nd–Fe–B sintered magnets; Coercivity; Demagnetization field

$(Nd_{0.7}Dy_{0.3})$–Fe–B sintered magnets with a maximum energy product, $(BH)_{max}$, of ~240 kJ m^{-3} and a coercivity, $\mu_0 H_c$, of ~3.0 T are currently used for the traction motors of hybrid vehicles. However, the scarcity of Dy discourages the continued use of Dy-substituted Nd–Fe–B magnets in the long term. Therefore, enhancing the coercivity of Nd–Fe–B permanent magnets and improving the temperature coefficient of coercivity must be achieved without substituting Dy for Nd [1].

One way to enhance the coercivity of Nd–Fe–B magnets is to refine the grain size [2–4]. The coercivity of Nd–Fe–B sintered magnets is known to exhibit a large grain size dependence following $H_c = a - b\ln D$ [2]. However, this relationship fails when the grain size is <3 μm because of the oxidation of Nd-rich phases in fine-grained sintered magnets [5]. Recently, Une and Sagawa demonstrated a high coercivity of 2 T using ultrafine-grained Nd–Fe–B sintered magnet ($D \approx 1$ μm) that was processed by controlling the oxygen atmosphere rigorously using the pressless sintering route [6]. The grain size reduction to ~1 μm showed not only a coercivity enhancement but also a two-step initial magnetization process from the thermally demagnetized stage to a magnetic saturation [6,7]. This raises questions, including: what is the mechanism by which the grain size reduction leads to an increase in coercivity? And why does the initial magnetization occur in two steps for fine-grained sintered magnets?

Ramesh et al. discussed the grain size dependence of the coercivity of sintered Nd–Fe–B magnets, assuming that the magnetic reversal occurs by nucleation in magnetically isolated grains, i.e., the coercivity increases as the grain size decreases due to the decrease in the defect density on the surface region [2]. However, recent detailed microstructural characterization of Nd–Fe–B sintered magnets has shown that the intergranular phase of sintered magnets is ferromagnetic, so the magnetic grains are exchange coupled [8,9]. Hence, the grain size dependence of the coercivity cannot be attributed to the reduction in defect densities in magnetically isolated $Nd_2Fe_{14}B$ grains, and must instead be explained by the magnetostatic field in an exchange-coupled polycrystalline model.

Finite-element micromagnetic simulations have been widely used to understand the influence of the microstructure of Nd–Fe–B permanent magnets on magnetic properties [10–19]. Simulations have demonstrated that the coercivity of anisotropic Nd–Fe–B magnets increases with decreasing grain size [13,18–19]. Micromagnetic simulations of a 2-D magnetic structure showed that in the large-grain-sized magnets, the $Nd_2Fe_{14}B$ grains are strongly coupled by long-range magnetostatic interactions which become less effective due to a decrease in the grain size leading to decrease in the demagnetization field [18]. However, no explicit explanation has been given for the grain size dependence of coercivity and the thermal stability of coercivity in Nd–Fe–B sintered

* Corresponding author; e-mail: h.sepehriamin@nims.go.jp

http://dx.doi.org/10.1016/j.scriptamat.2014.06.020
1359-6462/

magnets. This work uses finite-element micromagnetic simulations to understand the underlying mechanism of the grain size dependence of the coercivity of Nd–Fe–B sintered magnets. This study also addresses the reason for the change in the initial magnetization curves of ultrafine-grain-sized magnets and the dependence of the thermal stability of coercivity on grain size.

Models with polyhedral grains with average grain sizes of 0.7–2.7 μm were used to simulate the magnetization curves of Nd–Fe–B sintered magnets. The models were $8 \times 8 \times 8\ \mu m^3$ in size. The saturation magnetization ($\mu_0 M_s$), the magnetocrystalline anisotropy (K_1), and the exchange stiffness (A) of the $Nd_2Fe_{14}B$ phase were chosen to be 1.61 T, 4.5 MJ m^{-3}, and 12.5 pJm^{-1}, respectively [20]. Anisotropic $Nd_2Fe_{14}B$ grains (c-axis parallel to the Z direction) are considered to be weakly exchange coupled across grain boundaries with 2% exchange coupling strength of $Nd_2Fe_{14}B$ phase. Tetrahedral meshes were generated and the Landau–Lifshitz–Gilbert (LLG) equation was solved at each node by the FEMME software [15]. In these models, a large tetrahedral mesh size, around an order of magnitude larger than exchange length of $Nd_2Fe_{14}B$ phase, was used. Although this mesh size is much larger than exchange length of $Nd_2Fe_{14}B$ phase, the purpose of the simulation is to capture effect of magnetostatic interactions between the grains on the magnetization reversal. The coarse mesh may shift the computed nucleation fields to higher values. The change of the nucleation field with grain size is taken into account in a reduced order model with size of $400 \times 400 \times 400\ nm^3$ and a mesh size comparable to the exchange length of $Nd_2Fe_{14}B$ phase. To create an initial thermally demagnetized state, magnetic moments were randomly distributed and relaxed without an external magnetic field by finite-element micromagnetic (FEM) calculations. The magnetostatic interaction field is computed from a magnetic scalar potential. High accuracy is achieved through the use of a hybrid finite-element boundary method, in order to take into account the open boundary. The reliability of the method for computing the magnetostatic interactions in magnetic systems was demonstrated by the comparison of measured and calculated switching processes in magnetic nano-islands [21]. Magnetization curves were simulated by applying an external magnetic field.

The grain size of a cubic sample of $8 \times 8 \times 8\ \mu m^3$ was varied from 2.7 to 0.7 μm. Examples of the modeled geometries for average grain sizes of 1.0 and 2.7 μm are shown in Supplementary File 1. The simulated hysteresis curves of the models are shown in Figure 1a. Coercivity increases by 0.4 T when the grain size is decreased from 2.7 to 0.7 μm in the exchange-coupled models. The low initial susceptibility observed at magnetic field strengths below 1 T is due to the lack of time-relaxation in micromagnetic simulations, and this feature is not observed in experimental magnetization curves. Thus, we ignore the shape of the low initial susceptibility region observed in the micromagnetic simulations. This figure also demonstrates a decrease in maximum susceptibility as the grain size is reduced. For grain sizes >1 μm, the magnetization reaches saturation in one step. However, the initial magnetization does not reach saturation in one step for the 1 μm grain size sample, i.e., after reaching saturation, further application of a higher magnetic field is required

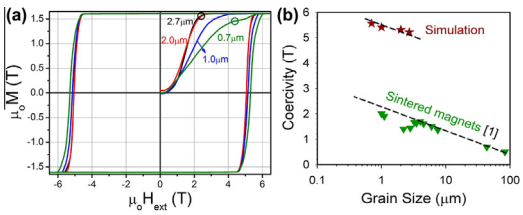

Figure 1. (a) Magnetization curves of the simulated magnets with average grain sizes of 2.7, 2.0, 1.0 and 0.7 μm. (b) Comparison of the coercivity vs. grain size obtained using micromagnetic simulations and experimentally reported Nd–Fe–B sintered magnets [1].

to reach saturation. In other words, the initial magnetization proceeds in two steps. This result is consistent with the recent experimental report describing a two-step initial magnetization curve for 1 μm grain sized sintered magnets [6,7]. In addition, the slopes of the demagnetization curves are also different for different grain sizes, i.e. abrupt magnetization reversals are observed at the nucleation fields for the 2.7 and 2 μm grain sizes, while gradual demagnetization after nucleation is observed for the 1 and 0.7 μm grain sizes. The coercivity as a function of grain size is shown in Figure 1b and is compared with the experimental results of sintered magnets [1]. Note that the unrealistically high coercivity in the simulation is mainly due to the ignorance of the defects that reduce the anisotropy field at surfaces and grain boundaries in real magnets. The grain size dependence of the coercivity in the simulation follows the same trend as the experimental observations.

Figure 2a,b shows the configuration of the magnetization of the modeled magnet, with an average grain size of 2.7 μm and an external magnetic field of 2.2 T (black circle in Fig. 1a) during the initial magnetization process. Note that the magnetic domains with upward and downward magnetization parallel to the Z direction are shown in red and blue in Figure 2a. For better visualization, only the magnetic domains with downward magnetization are shown in Figure 2b. Figure 2c,d shows the configuration of the magnetization of the modeled sample with an average grain size of 0.7 μm at an external magnetic field of 4.4 T (green circle in Fig. 1a). The $Nd_2Fe_{14}B$ grains in the model with a grain size of 2.7 μm are in the multidomain state, and domain walls can be observed within the $Nd_2Fe_{14}B$ grains. To better visualize the multidomain grains in the 2.7 μm grain size model, two grains are shown in Figure 2b. However, in the sample with a grain size of 0.7 μm, many $Nd_2Fe_{14}B$ grains are in the single domain state, in which no domain walls are observed within the $Nd_2Fe_{14}B$ grains. These observations indicate that the initial high susceptibility is due to the easy displacement of the magnetic domain walls within the multidomain $Nd_2Fe_{14}B$ grains. On the other hand, reversal of the magnetization of the single-domain particles required higher magnetic fields due to the pinning of the domain walls in the ~5 nm thick ferromagnetic grain boundary phase. This leads to the two-step magnetization process in the initial magnetization curve of the fine-grained Nd–Fe–B sintered magnets. Note that the two-step initial magnetization curves are observed in hot-deformed magnets, in which crystal grain size is comparable to the single-domain size of $Nd_2Fe_{14}B$ [22]. Hioki et al. reported

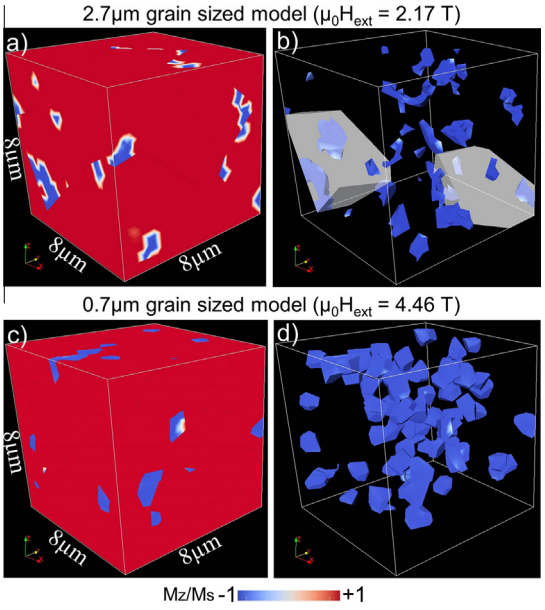

Figure 2. Magnetization configuration of thermally demagnetized models after applying magnetic fields of (a,b) 2.17 T to 2.7 μm grain sized magnets and (c,d) 4.46 T to 0.7 μm grain sized magnet. Note that (a) and (c) show the magnetization configuration at the surface of model while (b) and (d) only show domains with magnetization in the −Z direction.

that the fraction of magnetization in the high-susceptibility region corresponded to the volume fraction of the multidomain grains in the hot-deformed magnets [22].

In Nd–Fe–B sintered magnets, surface grains have almost no coercivity due to the defects created during surface machining/polishing [23] or due to the intrinsic nature of the (0 0 1) surface, i.e., negative crystal field parameters of the Nd ions on the (0 0 1) surface of $Nd_2Fe_{14}B$ [24]. Kerr microscopy observations of Nd–Fe–B bulk magnets show that magnetic domains are introduced on surface grains at a near zero field after saturation [25]. When the magnetization of the surface grains is reversed, the magnetically reversed surface grains cause stray fields in the underlying grains. The stray field generated from the reversed surface grains was calculated for different grain sizes as shown in Figure 3. Figure 3a shows the distribution of demagnetization vectors of 2.0 μm grain sized magnets. The magnetically reversed surface grains are shaded in Figure 3a. The arrows show the magnitude and direction of the stray field from the reversed grains. The distribution of the maximum stray field calculated from surface slices at Z = 0 μm to Z = 8 μm are plotted in Figure 3b. These data show that the largest stray field exists at the interfaces of the surface grains and that the largest value decreases as the grain size is decreased. Larger stray fields induce magnetization reversals of the neighboring grains at lower external magnetic fields, resulting in the dependence of grain size on coercivity.

One remaining question is how the grain size influences the temperature coefficient of coercivity, i.e., $\beta = [\Delta H_c/(H_c \Delta T)] \times 100$. Note that the typical value of β for commercial Nd–Fe–B sintered without Dy is $\sim -0.6\%\ °C^{-1}$. To enable the magnet to be used at elevated temperature, a low absolute value of β is desirable. As the models used

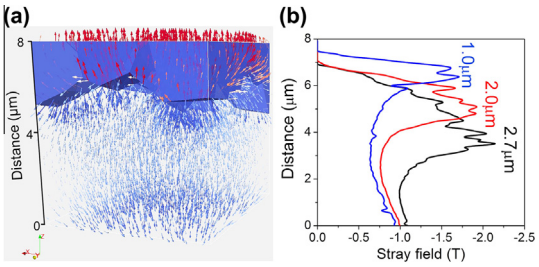

Figure 3. (a) Distribution of demagnetization vectors in the 2.0 μm grain sized model. Note that only surface grains have magnetization values of $M_z/M_s = -1$. (b) The distribution of the maximum stray field calculated from surface slices from Z = 0 μm to Z = 8 μm for models with grain sizes of 1.0, 2.0 and 2.7 μm.

in this paper are very large, a long calculation time is required to simulate coercivity vs. temperature. To enable calculations to be performed within reasonable periods of time, we reduced the model size to 400 × 400 × 400 nm^3 with polyhedral grains with average sizes of 30, 50 and 130 nm, two orders of magnitude smaller than commercial sintered magnets. Magnetization curves were calculated from 300 to 400 K in increments of 20 K. The materials parameters of $Nd_2Fe_{14}B$ phase for the calculation at T = 300–400 K were based on values measured by Hock [26]. Figure 4a shows the simulated coercivity vs. temperature for Nd–Fe–B models with grain sizes of 30, 50, and 130 nm and β was calculated for these models. The absolute value of β increases from 0.312% $°C^{-1}$ for a grain size of 30 nm to 0.337% $°C^{-1}$ for a grain size of 130 nm. This result suggests that the temperature coefficient of coercivity deteriorates with increasing grain size. This was also experimentally reported in hot-deformed Nd–Fe–B magnets [22].

Based on the nucleation model, the coercivity of Nd–Fe–B permanent magnets is often expressed as:

$$H_c[T] = \alpha H_a[T] - N_{eff} M_s[T]$$

in which the first term corresponds to the influence of microstructural defects on the anisotropy field and the second term corresponds to the microstructure-sensitive effective demagnetization [27]. By plotting H_c/M_s vs. H_A/M_s for different temperatures and applying a linear fit to the data, the values of α and N_{eff} are determined for Nd–Fe–B sintered magnets. Figure 4b shows the H_c/M_s vs. H_A/M_s of the modeled Nd–Fe–B magnets with average grain sizes of 30, 50 and 130 nm at different temperatures. The slopes of the plots do not change much and are nearly 1. This is because this model did not contain any defects. However, the effective demagnetization

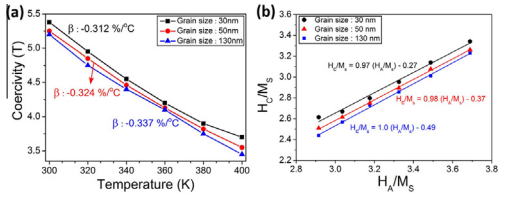

Figure 4. (a) Coercivity vs. temperature of modeled Nd–Fe–B magnets with average grain sizes of 30, 50 and 130 nm. (b) The dependence of H_c/M_s vs. H_A/M_s of the modeled samples with average grain sizes of 30, 50 and 130 nm. The micromagnetic parameters of α and N_{eff} are measured from the slope and intercept, respectively, of a linear fit to this graph.

constant, N_{eff}, increases from 0.27 for a grain size of 30 nm to 0.49 for a grain size of 130 nm. This result suggests that the effective local demagnetization factor increases as the grain size increases. In fact, this is consistent with the stray field calculation shown in Figure 3.

The thermal degradation of coercivity is known to be improved by the reduction of the grain size in Nd–Fe–B permanent magnets [1]. The present micromagnetic simulation result is consistent with experimental results. However, the underlying mechanism of this phenomenon has not been explicitly explained in previous studies. Increasing the temperature from room temperature results in a decrease in both the anisotropy field and the saturation magnetization of the $Nd_2Fe_{14}B$ phase [28]. However, the saturation magnetization and anisotropy field do not decrease at the same rate. The anisotropy field decreases from room temperature to ~200 °C with a sharp negative slope. However, the saturation magnetization decreases at a much slower rate from room temperature to ~160 °C [28]. Thus, the $N_{eff}M_s$ term in the micromagnetic model is less temperature dependent than αH_A at elevated temperatures. The $N_{eff}M_s$ term will compensate for the αH_A term as was addressed by Kronmüller and Fähnle [29]. Thus, lower values for $N_{eff}M_s$ suppress the thermal degradation of the coercivity. The micromagnetic simulation results (Fig. 4) show that N_{eff} decreases with decreasing grain size. Thus, the effect of the stray field is smaller at elevated temperature, explaining the better thermal stability of coercivity for smaller-grained Nd–Fe–B permanent magnets.

Using micromagnetic simulations for polycrystalline anisotropic magnets, we have shown that only the stray field decreases as the grain size is decreased. Once a reversed domain is nucleated from an area with low local anisotropy such as the surface or interface with non-ferromagnetic inclusions, magnetization reversal propagates to neighboring grains through ferromagnetic grain boundary phases. The shape of the demagnetization curve (Fig. 1a) in the model with a grain size of 2.7 μm showed a sharp reduction in magnetization at the nucleation field. This result suggests that the grain boundaries exert only a weak pinning force against magnetic domain wall motion. However, by reducing the grain size, the difference of nucleation field and coercivity becomes larger, potentially due to the increase in pinning sites such as grain boundaries.

In summary, micromagnetic simulations qualitatively reproduce the experimentally observed grain size dependence of coercivity in weakly exchange coupled anisotropic Nd–Fe–B sintered magnets with grain sizes ranging from 2.7 to 0.7 μm. The increase in coercivity with decreasing grain size is attributed to the reduction in the stray field arising from neighboring grains. The shape of the initial magnetization curves was found to change from a one-step magnetization process resulting from domain wall displacement to a two-step process involving domain wall displacement within multidomain grains and domain wall pinning at the soft magnetic grain boundary phase into single-domain grains. The micromagnetic simulation results also explain the grain size dependence of the temperature coefficient of coercivity, i.e., the lower effective demagnetization constant, N_{eff}, suppresses the temperature degradation of coercivity.

This work was supported by the Japan Science and Technology Agency (JST), CREST.

Supplementary data associated with this article can be found, in the online version, at http://dx.doi.org/10.1016/j.scriptamat.2014.06.020.

[1] K. Hono, H. Sepehri-Amin, Scripta Mater. 67 (2012) 530.
[2] R. Ramesh, K. Srikrishna, J. Appl. Phys. 64 (1988) 6406.
[3] P. Nothnagel, K.H. Müller, D. Eckert, A. Handstein, J. Magn. Magn. Mater. 101 (1991) 379.
[4] K. Uestuener, M. Katter, W. Rodewald, IEEE Trans. Magn. 42 (2006) 2897.
[5] W.F. Li, T. Ohkubo, K. Hono, M. Sagawa, J. Magn. Magn. Mater. 321 (2009) 1100.
[6] Y. Une, M. Sagawa, in: Presented at REPM'10, Bled, Slovenia, 2010.
[7] H. Sepehri-Amin, Y. Une, T. Ohkubo, K. Hono, M. Sagawa, Scripta Mater. 65 (2011) 396.
[8] H. Sepehri-Amin, T. Ohkubo, T. Shima, K. Hono, Acta Mater. 60 (2012) 819.
[9] Y. Murakami, T. Tanigaki, T.T. Sasaki, Y. Takeno, H.S. Park, T. Matsuda, T. Ohkubo, K. Hono, D. Shindo, Acta Mater. 71 (2014) 370.
[10] T. Schrefl, J. Fidler, J. Magn. Magn. Mater. 111 (1992) 105.
[11] T. Schrefl, R. Fischer, J. Fidler, H. Kronmüller, J. Appl. Phys. 76 (1997) 7053.
[12] G. Hrkac, T.G. Woodcock, K.T. Butler, L. Saharan, M.T. Bryan, T. Schrefl, O. Gutfleisch, Scripta Mater. 70 (2014) 35.
[13] J. Fidler, T. Schrefl, J. Appl. Phys. 79 (1996) 5029.
[14] H. Kronmüller, R. Fischer, R. Hertel, T. Leineweber, J. Magn. Magn. Mater. 175 (1997) 177.
[15] J. Fidler, T. Schrefl, J. Phys. D: Appl. Phys. 33 (2000) R135.
[16] D. Süss, T. Schrefl, J. Fidler, IEEE Trans. Magn. 36 (2000) 3282.
[17] D.C. Crew, Er. Girt, D. Suess, T. Schrefl, K.M. Krishnan, G. Thomas, M. Guilot, Phys. Rev. B 66 (2002) 184418.
[18] T. Schrefl, H.F. Schmidts, J. Fidler, H. Kronmüller, IEEE Trans. Magn. 29 (1993) 2878.
[19] H.F. Schmidts, H. Kronmüller, J. Magn. Magn. Mater. 94 (1991) 220.
[20] M. Sagawa, S. Fujimura, H. Yamamoto, T. Matsuura, S. Hirosawa, J. Appl. Phys. 57 (1985) 4094.
[21] C.M. Günther, O. Hellwig, A. Menzel, B. Pfau, F. Radu, D. Makarov, M. Albrecht, A. Goncharov, T. Schrefl, W.F. Schlotter, R. Rick, J. Lüning, S. Eisebitt, Phys. Rev. B 81 (2010) 064411.
[22] K. Hioki, Y. Kojima, T. Morita, A. Hattori, in: Presented at IEEE International Magnetics Conference, Vancouver, Canada, 2012.
[23] S. Hirosawa, K. Tokuhara, M. Sagawa, Jpn. J. Appl. Phys. 26 (1987) L1359.
[24] H. Moriya, H. Tsuchiura, A. Sakuma, J. Appl. Phys. 105 (2009) 07A740.
[25] K. Kobayashi, K. Itoh, D. Shimizu, K. Hayawaka, M. Sagawa, J. Mag, J. Magn. Soc. Jpn. 31 (2007) 393.
[26] S. Hock, (Ph.D. thesis), University of Stuttgart, 1988.
[27] K.-D. Durst, H. Kronmüller, J. Magn. Magn. Mater. 68 (1987) 63.
[28] S. Hirosawa, Y. Matsuura, H. Yamamoto, S. Fujimura, M. Sagawa, H. Yamauchi, J. Appl. Phys. 59 (1986) 873.
[29] H. Kronmüller, M. Fähnle, in: Micromagnetism and the Microstructure of Ferromagnetic Solids, Cambridge University Press, Cambridge, 2003, p. 123.